NASA Technical Memorandum 107143
AIAA–96–0871

Wind Tunnel Measured Effects on a Twin-Engine Short-Haul Transport Caused by Simulated Ice Accretions

Andrew Reehorst, Mark Potapczuk, and Thomas Ratvasky
Lewis Research Center
Cleveland, Ohio

Brenda Gile Laflin
Langley Research Center
Hampton, Virginia

Prepared for the
34th Aerospace Sciences Meeting and Exhibit
sponsored by the American Institute of Aeronautics and Astronautics
Reno, Nevada, January 15–18, 1996

National Aeronautics and
Space Administration

WIND TUNNEL MEASURED EFFECTS ON A TWIN-ENGINE SHORT-HAUL TRANSPORT CAUSED BY SIMULATED ICE ACCRETIONS

by:
Andrew Reehorst
Mark Potapczuk
Thomas Ratvasky

NASA Lewis Research Center
Cleveland, Ohio

Brenda Gile Laflin

NASA Langley Research Center
Hampton, Virginia

Abstract

A series of wind tunnel tests were conducted to assess the effects of leading edge ice contamination upon the performance of a short-haul transport. The wind tunnel test was conducted in the NASA Langley 14 by 22 foot facility. The test article was a 1/8 scale twin-engine short-haul jet transport model. Two separate leading edge ice contamination configurations were tested in addition to the uncontaminated baseline configuration. Several aircraft configurations were examined including various flap and slat deflections, with and without landing gear. Data gathered included force measurements via an internal six-component force balance, pressure measurements through 700 electronically scanned wing pressure ports, and wing surface flow visualization measurements. The artificial ice contamination caused significant performance degradation and caused visible changes demonstrated by the flow visualization. The data presented here is just a portion of the data gathered. A more complete data report is planned for publication as a NASA Technical Memorandum and data supplement.

Nomenclature

b	wing span, feet
c_s	slat chord length, feet
c_w	wing main element chord length, feet
c_{ff}	forward flap element chord length, feet

c_{mf} mid flap element chord length, feet

c_{af} aft flap element chord length, feet

c_p pressure coefficient, $(p_n-p_{atm})/q$

C_D drag coefficient, Drag/qS

C_L lift coefficient, Lift/qS

C_m pitching moment coefficient, pitching moment/qSb

p_{atm} atmospheric pressure, lb/ft^2

p_n pressure at specific model tap n=1,2..., lb/ft^2

q free-stream dynamic pressure, lb/ft^2

S wing area, ft^2

a angle of attack, deg

b sideslip angle, deg

d_f flap deflection angle, deg

Introduction

Aircraft icing simulation methods are currently under development in order to provide design and certification tools for the aircraft industry. These tools include simulation methods for ice accretion, ice protection system performance, and aircraft performance degradation, and scaling methods. As in all computer simulations of physical processes, it is important to determine the quality of the prediction. This paper presents results of an experimental program designed to provide validation information for performance degradation of a commercial transport aircraft with ice accumulated on its wing and tail.

It is important to understand how ice accretions can influence the aerodynamic behavior of an aircraft in order to determine the ice protection requirements and to understand the effects of an ice protection system failure. This is currently done through flight and wind tunnel tests using real or artificial ice accretions. The development of a reliable computational tool for evaluation of performance changes due to ice accretion would help to decrease the number of such tests and in turn reduce the time and costs of design and certification.

The need for a computational tool and validation database is based on the desire of several aircraft manufacturers to determine the size and shape of ice accretions which are critical to aerodynamic performance. Currently, there is not a great deal of such data publicly available for a complete aircraft with ice. There have been several studies of airfoil and wing models with leading edge ice accretions[1-3]. These have provided information of sufficient quality to assess the accuracy of computational simulations and have helped to point out areas for improvement of such simulation methods. The data from this test program should serve a similar purpose for the evaluation of simulation methods applied to complete aircraft configurations.

Test Apparatus

The wind tunnel test was conducted in the NASA Langley 14 by 22 foot

subsonic wind tunnel. The test article for the test was a 1/8 scale twin-engine short-haul jet transport model. Several aircraft configurations were examined including various flap and slat deflections, with and without landing gear. Two separate configurations of leading edge ice contamination were tested in addition to the uncontaminated baseline configuration.

Facility Description

The NASA Langley 14 by 22 foot Subsonic Tunnel[4] is a closed-circuit, single return, atmospheric wind tunnel with a test section that can be operated in a variety of configurations: closed, slotted, partially open, and open. For this test, the test section was operated in the closed configuration. The closed test section is 14.5 feet high by 21.75 feet wide by 50 feet long.

Model Description

The model used for this test was a 1/8 scale twin-engine subsonic transport with multi-element wings[5] shown in figure 1. The empennage consisted of a vertical tail with rudder and a motorized horizontal stabilizer with elevator. The engines were represented by two flow-through nacelles. The model was tested in cruise, take-off, and landing configurations.

Ice shape description

Two different artificial ice shapes were used for this test. They were based upon drawings of ice shapes used by Boeing for a mid 1960s wind tunnel test of a similar aircraft[6]. The two shapes represent realistically sized ice accretions for this configuration. Because of the age of the information, no clear documentation was identified stating the method of determining these shapes, however, it is conjectured that the shapes were developed using either the Boeing ice shape prediction technique[7] or the method described in the FAA icing handbook[8].

The Boeing outlines were transformed to provide the appropriate scale and orientation for production of the artificial ice shapes in the NASA Lewis Research Center's wood-model shop. The ice shapes were manufactured for inboard and outboard wing, vertical tail and horizontal tail surfaces for both sides of the aircraft. The ice shapes were attached to the aircraft model using mechanical fasteners and double sided adhesive tape. Figures 2 and 3 show the artificial ice shapes attached to the horizontal tail. After being attached, the joints between the aircraft model and the ice shapes were filled using modeling clay. Profiles of the ice shapes installed on the aerodynamic surfaces were measured after the test to document the ice shapes used and their alignment to the aircraft surfaces.

Roughness determination

The roughness size for the model ice shapes was calculated by scaling down experimentally measured roughness. Roughness elements have been measured in the NASA Lewis Icing Research Tunnel and have been determined to be on the order of 0.02 inches[9,10]. This approximate value does not appear to vary significantly as the chord length or airfoil section changes, and is therefore considered reasonable for the full scale transport ice accretion. The next step in calculating the model ice roughness

size was to determine an appropriate scaling method. Neither full scale roughness nor geometrically scaled roughness are appropriate, since neither will appropriately address the change in the flow field due to the presence of roughness. The method selected was to scale the roughness with the ratio of the model to full scale boundary layer momentum thicknesses. The momentum thickness was calculated for both the full scale and 1/8 scale ice shapes using Cebeci's IBL computer program[11,12]. The average ratio between the two momentum thickness was 0.5411. When the full scale roughness size of 0.02 inches is multiplied by the scaling ratio of 0.5411, the scale model roughness size becomes 0.011 inches. This corresponds to a roughness that falls between a #60 and #70 grit. #60 grit, with nominal 0.0117 inch diameters, was utilized for this experiment. Figure 4 is a close-up view of the grit applied to the artificial ice shape.

Test Procedures

The test was conducted at dynamic pressures, q, from 10 lb/ft^2 to 50 lb/ft^2 corresponding to Reynolds numbers of 8.2×10^5 to 1.8×10^6 and Mach numbers of 0.08 to 0.18. Data was obtained over an angle-of-attack range from -4^o through 16^o with sideslip varying from -10^o to 10^o.

Aerodynamic forces and moments were obtained with a six-component strain-gauge balance and wing pressures were obtained with electronically scanned pressure devices from flush pressure ports. Angle-of-attack and sideslip were measured electronically in the model/model support system. Wing, body and wake blockage corrections to free stream dynamic pressure[13] were applied as were corrections for tunnel wall interference[14].

Two different flow visualization techniques were utilized during this test. The first technique was a surface oil method that utilized motor oil with a fluorescent additive viewed under ultraviolet lighting. The oil was painted on the left wing surface in a span-wise direction. When the proper test condition was achieved an overhead photograph was quickly taken with an ultraviolet flash. Due to the restrictive nature of this testing technique, only a select number of model configurations were examined with this technique.

A less restrictive technique was utilized for almost all test conditions. This technique makes use of fluorescent mono-filament wing tufts glued to the left wing. The tufts were digitally photographed using an ultraviolet flash. The "mini-tufts" do not provide quite the image resolution of the oil flow visualization technique, but proved to be much more practical for regular use since they required little upkeep from one test condition to the next.

Results

The lift, moment and drag coefficients are shown in figure 5 for the 40^o flap deflection model configuration with the uncontaminated leading edge and the #2 ice shape attached to various surfaces. The lift and pitching moment are clearly influenced by the presence of ice contamination on the outboard wing, but seem to be rather insensitive to the presence of ice on the horizontal tail.

Figures 6 through 9 show the chord-wise wing pressure coefficient

distributions for the various instrumented span-wise locations of the right model wing for both the clean and leading edge ice-contaminated configurations. The influence of leading edge ice contamination on the pressure distributions of the wing is particularly evident in figures 7 and 8 (10^{o} and 13^{o} angle-of-attack, respectively), visible to a lesser degree in figure 9 (15^{o} angle-of-attack), and nearly indiscernible in figure 6 (6^{o} angle-of-attack). The varying differences can be explained by examining the oil flow visualization data.

The oil flow visualization images shown in figures 10 through 21 help explain the behavior seen in the wing pressure distribution data. Figures 10 and 11 (0^{o} angle-of-attack) show no visible difference in the wing flow patterns between the clean and contaminated configurations. Flows in both cases appear to be completely attached. Figures 12 and 13 (8^{o} angle-of-attack) show only a small difference in the wing tip region. Beginning with figures 14 and 15 (10^{o} angle-of-attack) a more significant difference in the two flow patterns becomes visible. The flow is clearly beginning to separate at about the half span point on the contaminated wing. Moving to figures 16 and 17 (12^{o} angle-of-attack) the separated region on the contaminated wing becomes even more significant, with a large portion of the wing demonstrating detached flow. This separated region gets larger as the angle-of-attack is increased to 13^{o} in figures 18 and 19. And it is not until 15^{o} angle-of-attack (figures 20 and 21) that the clean wing begins to demonstrate separated flow. Referring back to figure 5, the flow visualization images do a good job of explaining the differences seen in the various plots, particularly in the coefficient of lift plot. The flow visualization images also support the wing pressure data in figures 6 through 9.

This series of force, moment, and pressure data and flow visualization images is representative of the data and the trends seen for the entire test.

Conclusions

Wind tunnel tests examining the effects of leading edge ice contamination upon the performance of a short-haul transport were discussed. Data gathered included force measurements, wing pressure measurements, and wing surface flow visualization measurements. As demonstrated by the flow visualization, the artificial ice contamination caused notable flow changes which resulted in significant performance degradations. Due to constraints of practical publication, the data presented here is just a small portion of data gathered. A much larger data report is planned for publication in the near future as a NASA Technical Memorandum and data supplement. This will represent the first major database of icing effects with a full aircraft configuration for code validation available in the public domain.

Acknowledgments

The authors would like to thank the efforts of the craftsmen in the NASA Lewis Research Center's wood-model shop, the engineers and technicians at the NASA Langley Research Center's 14x22 foot wind tunnel, and especially Mike Schura for assistance in determining the ice shapes to be

examined. Without their assistance, this wind tunnel test would not have been possible.

References

1. Bragg, M.B. and Spring, S.A., "An Experimental Study of the Flow Field about an Airfoil with Glaze Ice," AIAA Paper 87-0100, Jan. 1987.

2. Khodadoust, A. and Bragg, M.B.,"Measured Aerodynamic Performance of a Swept Wing with a Simulated Ice Accretion," AIAA Paper 90-0490, Jan. 1990.

3. Flemming, R.J., Britton, R.K., and Bond, T.H., "Model Rotor Icing Tests in the NASA Lewis Icing Research Tunnel," AGARD Conference Proceedings 496, Paper No. 9, Dec. 1991.

4. Gentry, Garl L. Jr., Quinto, P. Frank, Gatlin, Gregory M., and Applin, Zachary T.,"The Langley 14- by 22-Foot Subsonic Tunnel: Description, Flow Characteristics, and Guide for Users",NASA TP 3008, September 1990.

5. Paulson, John P.,"Wind-Tunnel Results of the Aerodynamic Characteristics of a 1/8-Scale Model of a Twin-Engine Short-Haul Transport", NASA TM X-74011, April 1977.

6. Hill, Eugene G., Personal communication, November 1992.

7. Wilder, Ramon, W.,"A theoretical and experimental means to predict ice accretion shapes for evaluating aircraft handling and performance characteristics", Paper 5, AGARD Advisory Report No. 127, September 1977.

8. Bowden, D.T., Gensemer, A.G., and Sheen, C.A.,"Engineering Summary of Airframe Icing Technical Data, FAA Technical Data, FAA Technical Report ADS-4, December 1963.

9. Hansman, R. John,"Analysis of Surface Roughness Generation in Aircraft Ice Accretion", AIAA-92-0298, January 1992.

10. Shin, Jaiwon,"Characteristics of Surface Roughness Associated with Leading Edge Ice Accretion",AIAA-94-0799, NASA TM-106459, January 1994.

11. Cebeci, T. and Chang, K.C.,"Calculation of Incompressible Rough-Wall Boundary-Layer Flows",AIAA Journal, Vol. 16, No. 7, July 1978.

12. Cebeci, T., Clark, R.W., Chang, K.C., Halsey, N.D. and Lee, K.,"Airfoils with Separation and the Resulting Wakes",Journal of Fluid Mechanics, Vol. 163, pp. 320-347, 1986.

13. Heyson, Harry H.,"Use of Superposition in Digital Computers to Obtain Wind-Tunnel Interference Factors for Arbitrary Configurations, With Particular Reference to V/STOL Models", NASA TR R-302, February 1969.

14. Rae, W.H., Jr., and Pope, A, Low-Speed Wind Tunnel Testing, John Wiley & Sons, Inc., 1984.

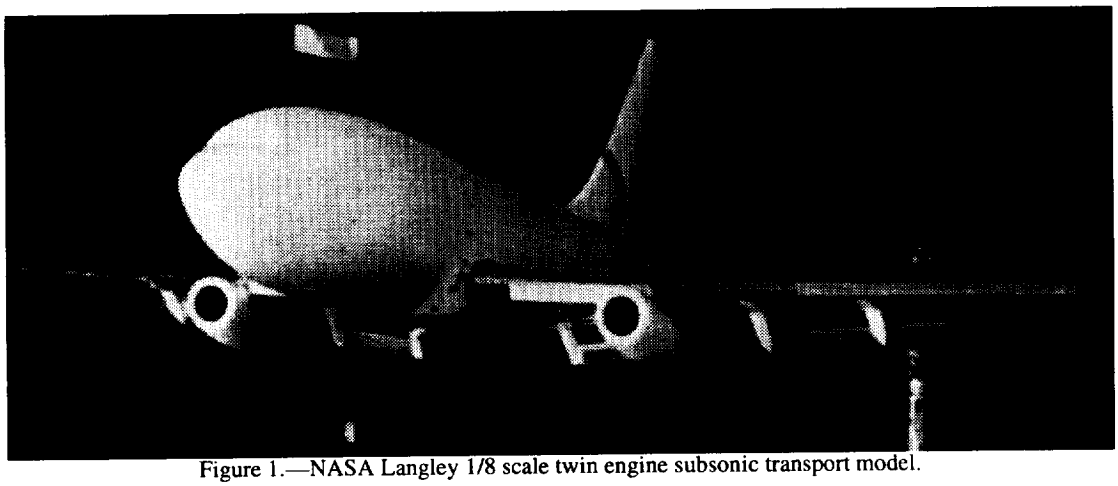

Figure 1.—NASA Langley 1/8 scale twin engine subsonic transport model.

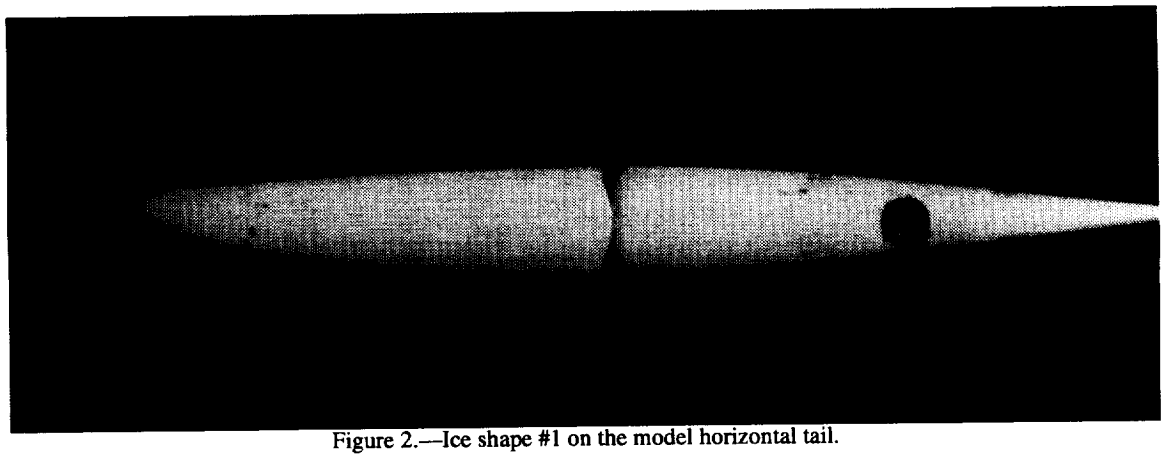

Figure 2.—Ice shape #1 on the model horizontal tail.

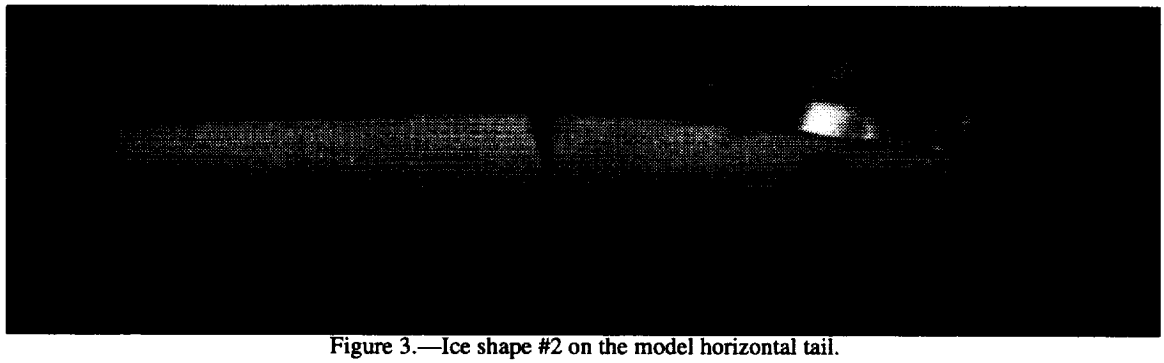

Figure 3.—Ice shape #2 on the model horizontal tail.

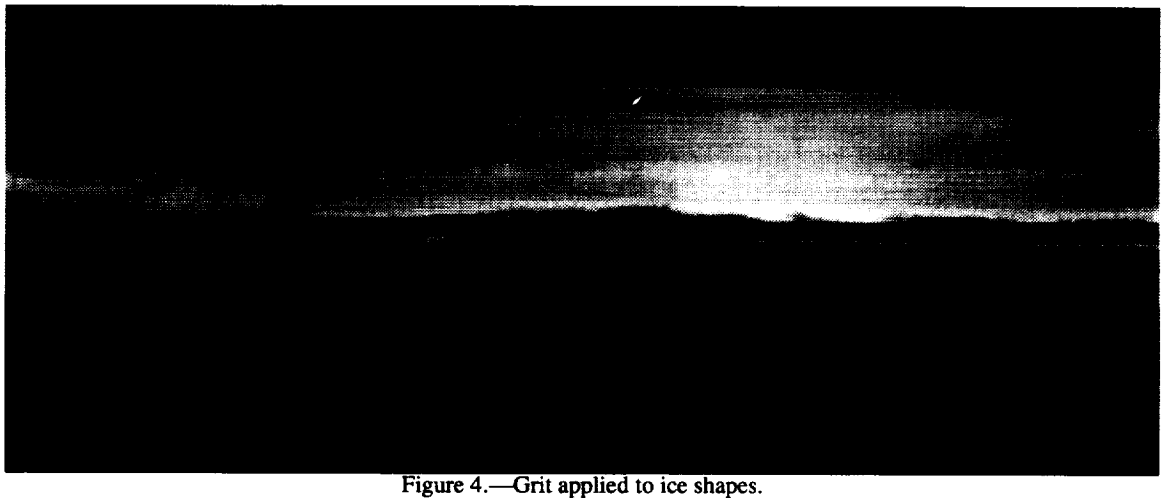

Figure 4.—Grit applied to ice shapes.

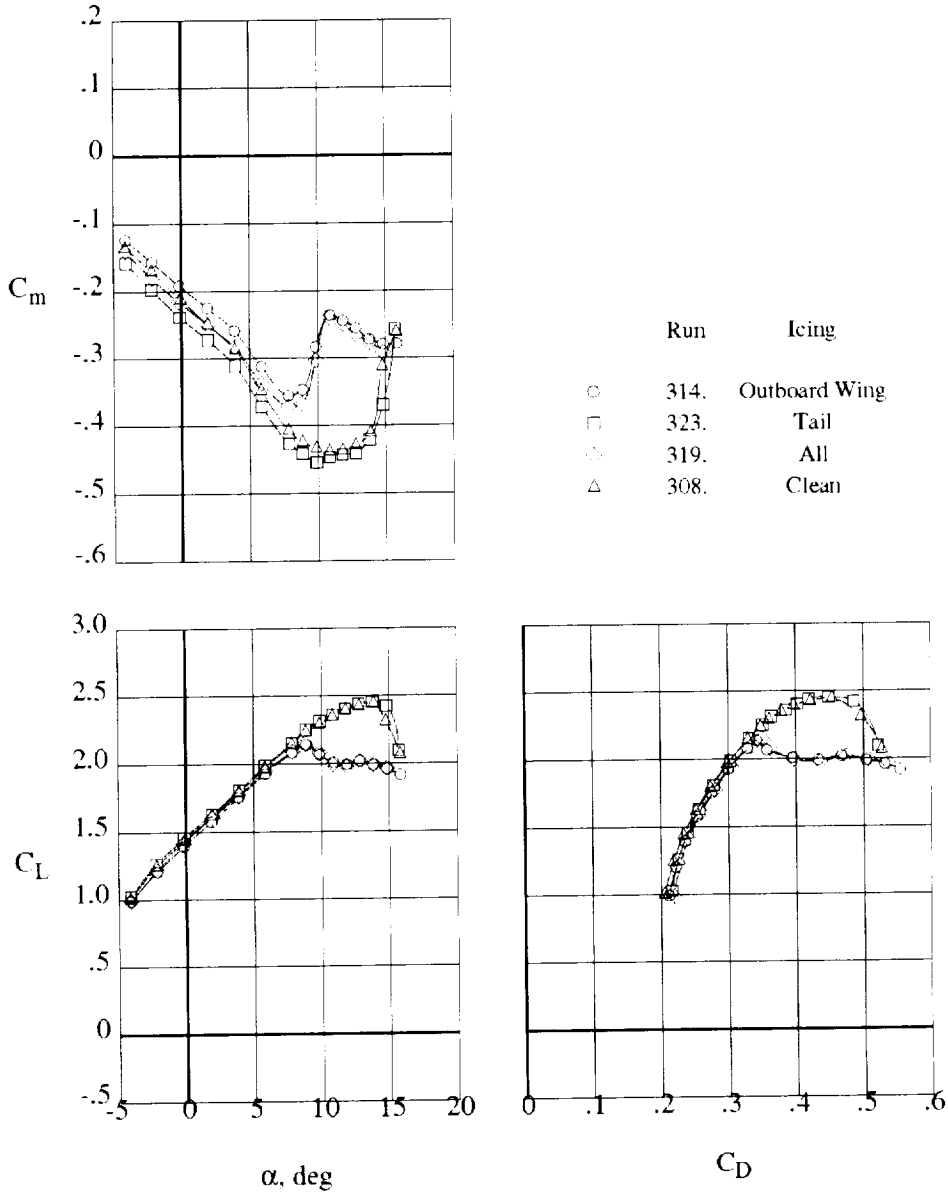

Figure 5.—Effects of Ice #2 on longitudinal aerodynamic characteristics of the model in the d_f=40° configuration.

	Run	Icing
○	314.	Outboard Wing
□	308.	Clean

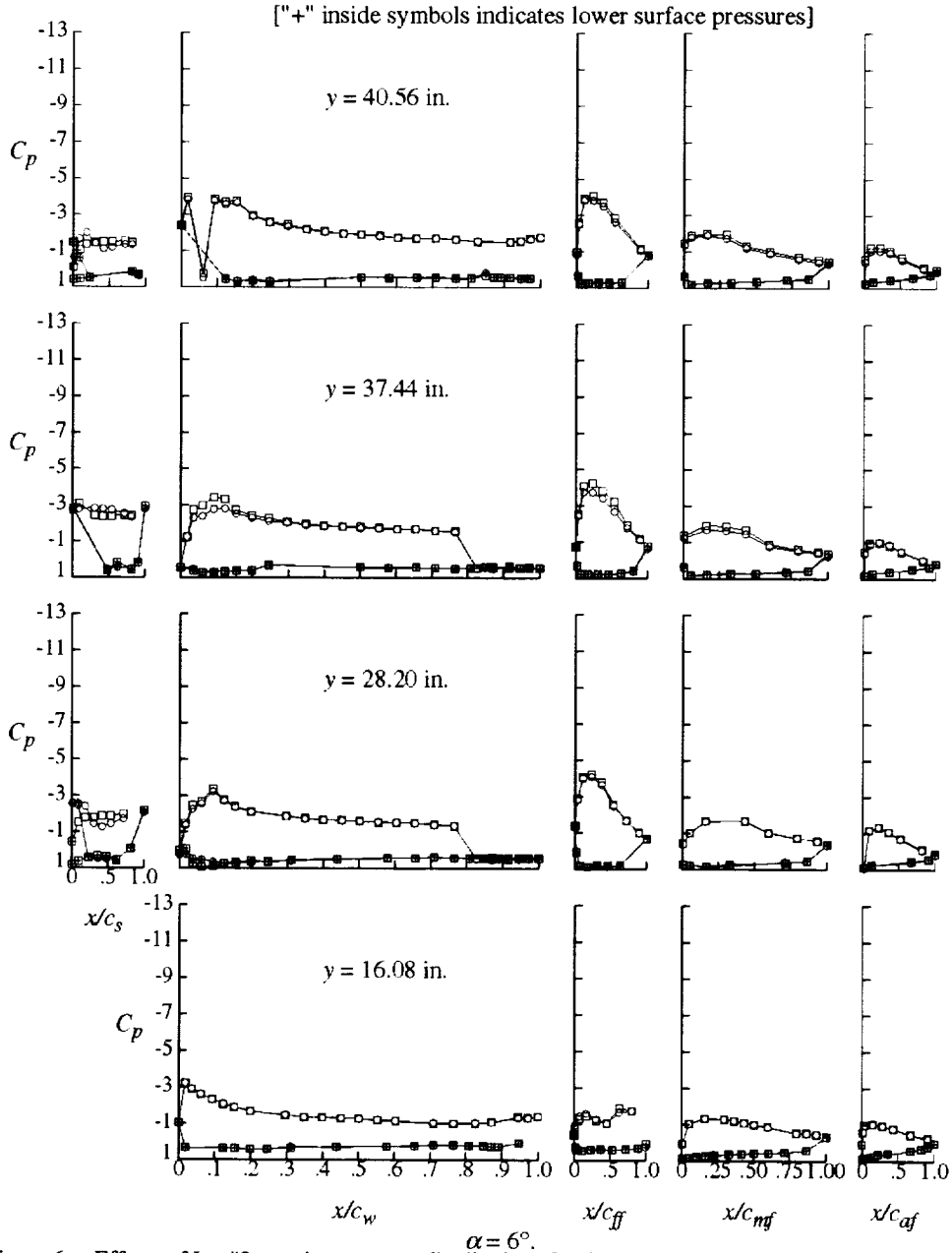

Figure 6.—Effects of Ice #2 on wing pressure distributions for the model in the d_f=40° configuration.

	Run	Icing
○	314.	Outboard Wing
□	308.	Clean

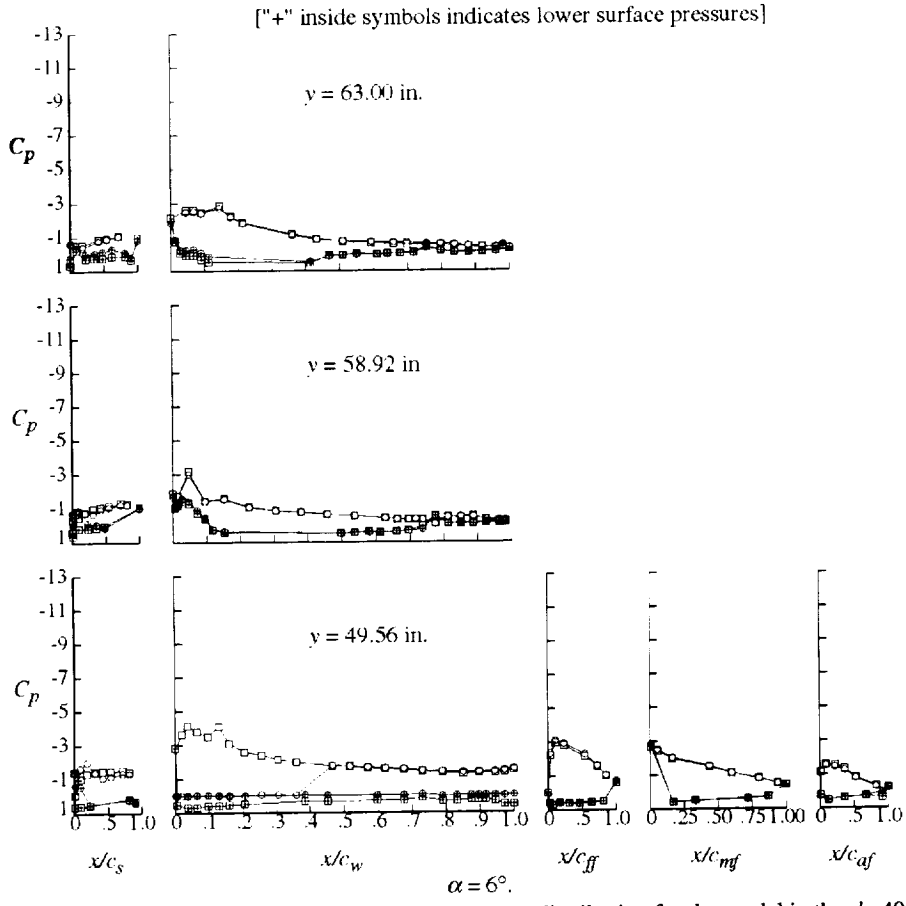

Figure 6 (concluded).—Effects of Ice #2 on the wing pressure distribution for the model in the d_f=40° configuation.

○	314.	Outboard Wing
□	308.	Clean

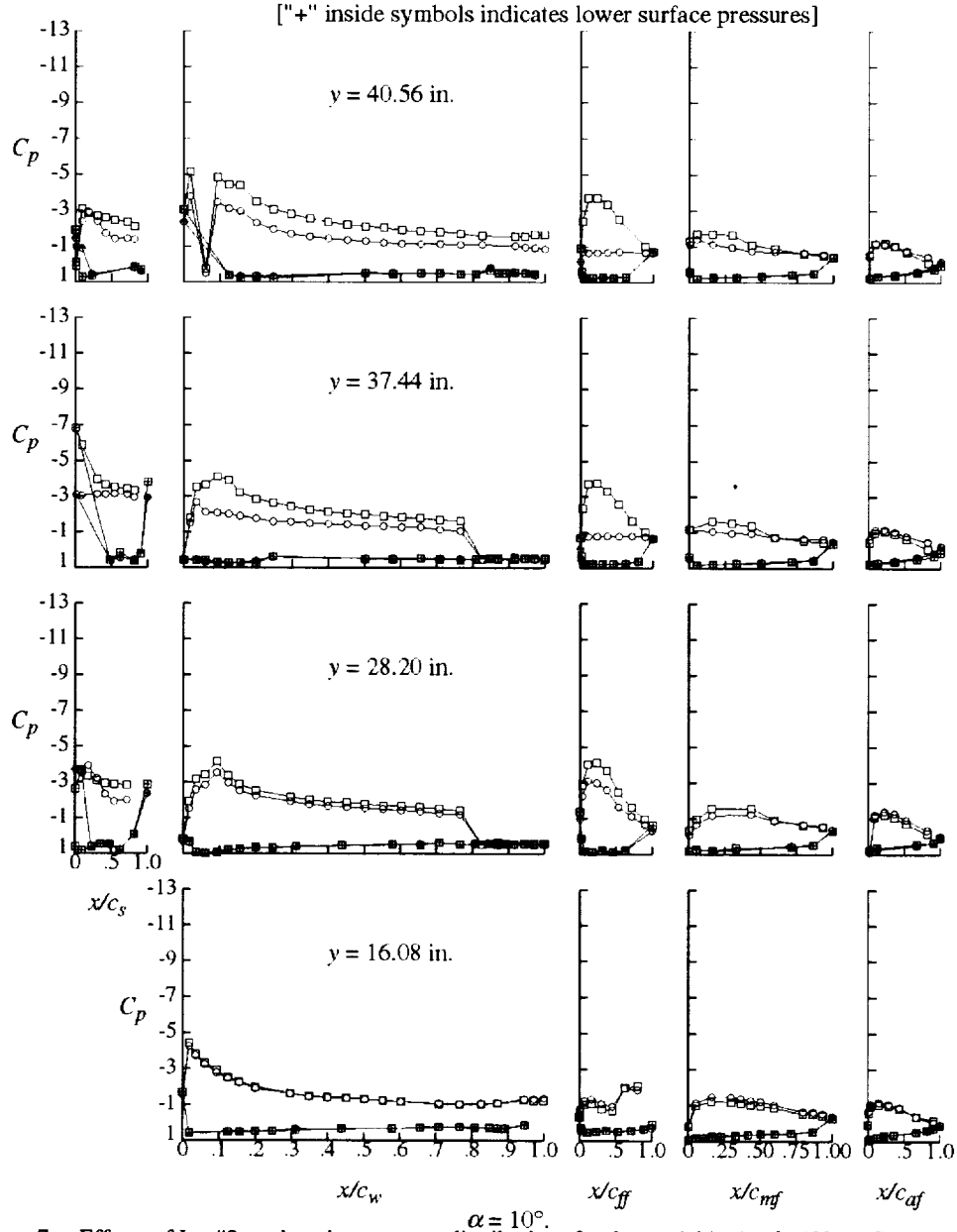

Figure 7.—Effects of Ice #2 on the wing pressure distributions for the model in the d_f=40° configuration.

	Run	Icing
○	314.	Outboard Wing
□	308.	Clean

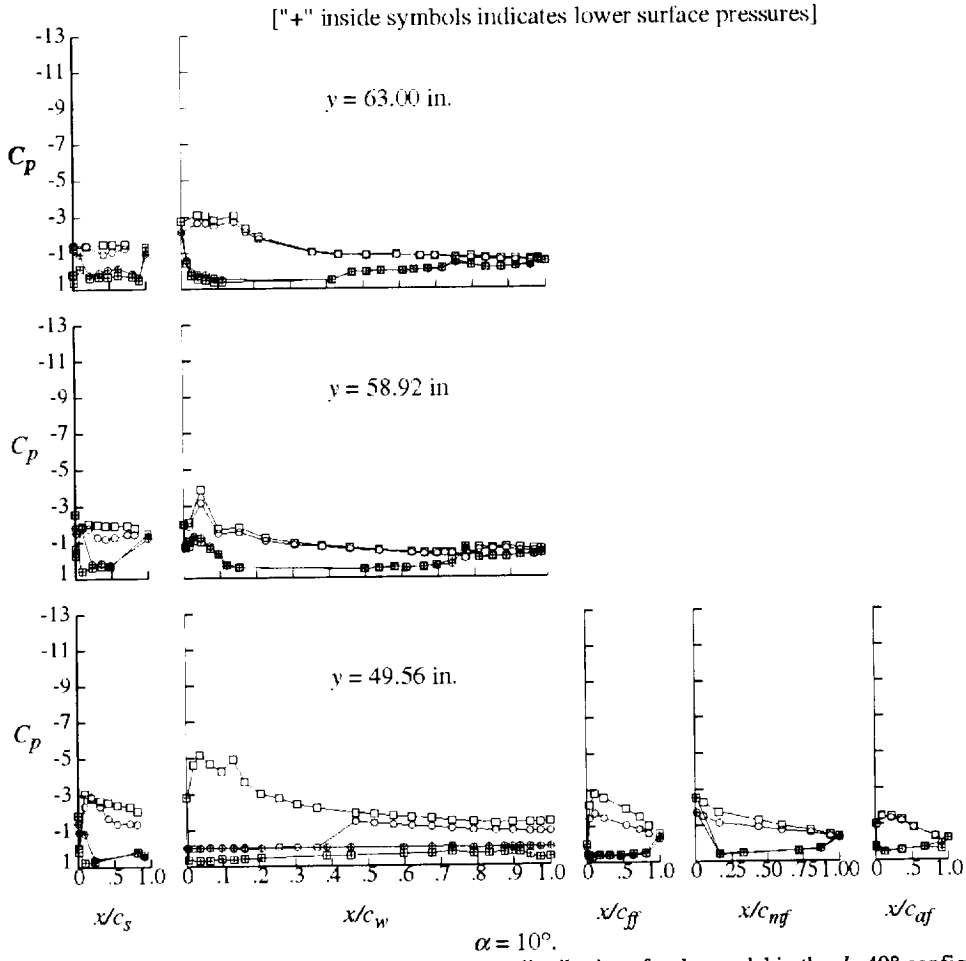

Figure 7 (concluded).—Effects of Ice #2 on the wing pressure distributions for the model in the d_f=40° configuration.

	Run	Icing
○	314.	Outboard Wing
□	308.	Clean

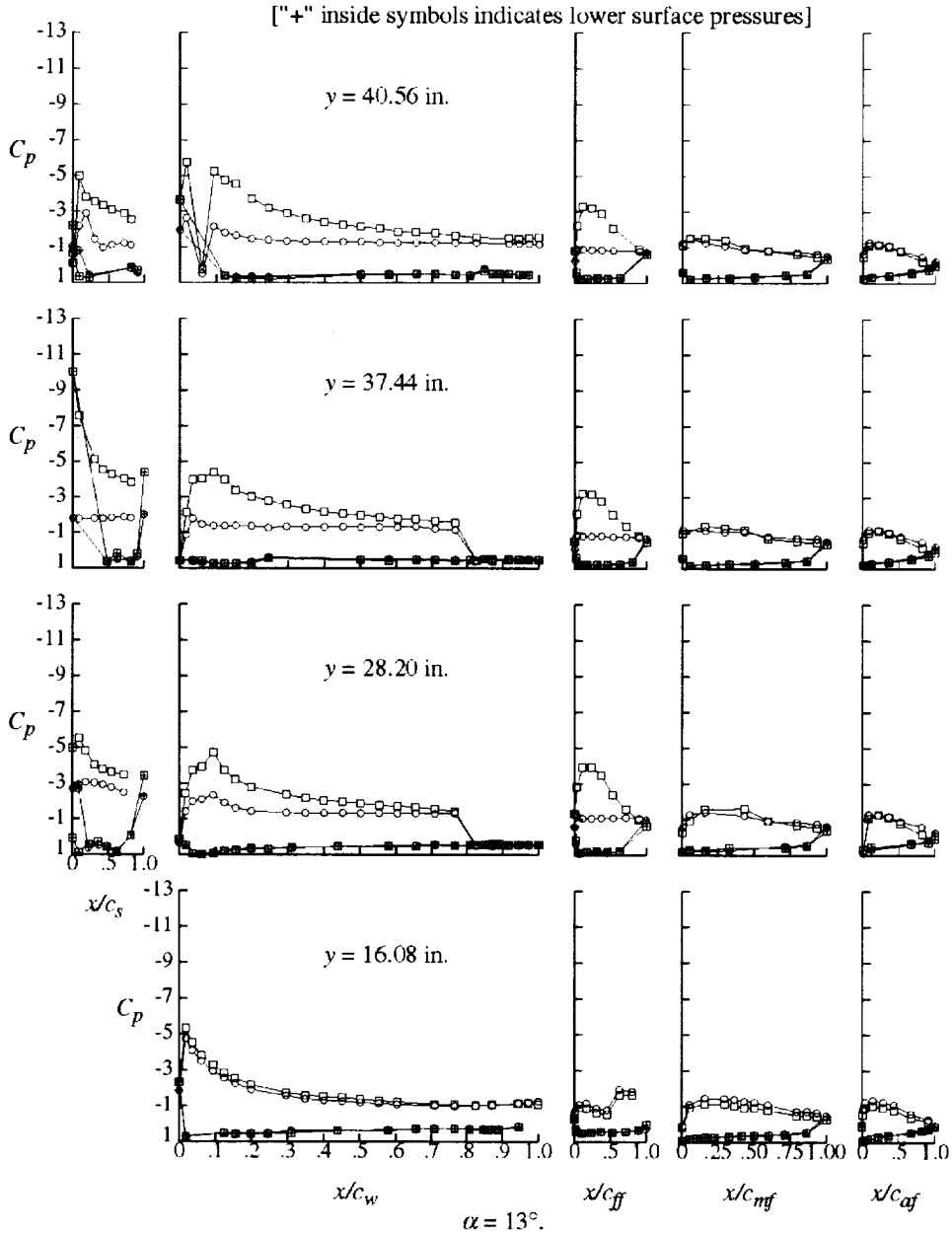

Figure 8.—Effects of Ice #2 on the wing pressure distributions for the model in the d_f=40° configuration.

	Run	Icing
○	314.	Outboard Wing
□	308.	Clean

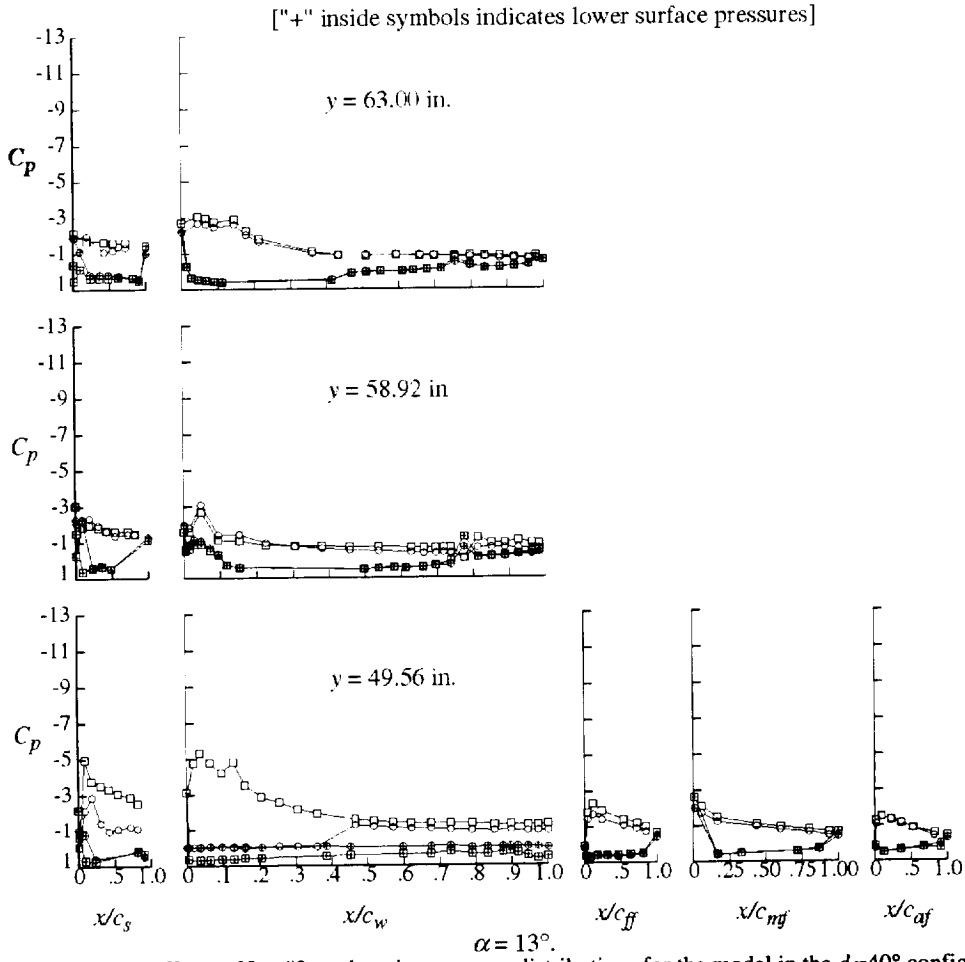

Figure 8 (concluded).—Effects of Ice #2 on the wing pressure distributions for the model in the d_f=40° configuration.

	Run	Icing
○	314.	Outboard Wing
□	308.	Clean

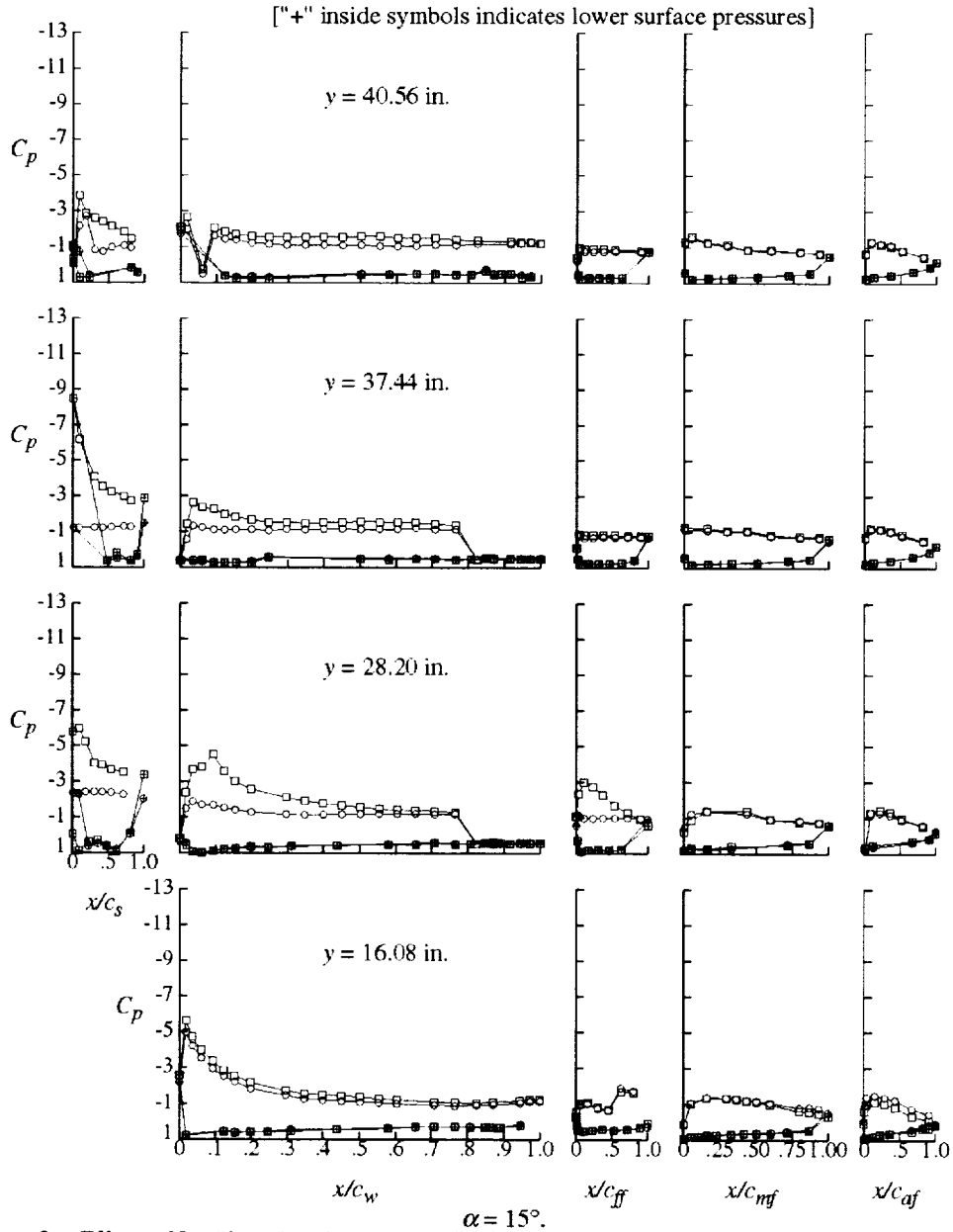

Figure 9.—Effects of Ice #2 on the wing pressure distributions for the model in the d_f=40° configuration.

	Run	Icing
○	314.	Outboard Wing
□	308.	Clean

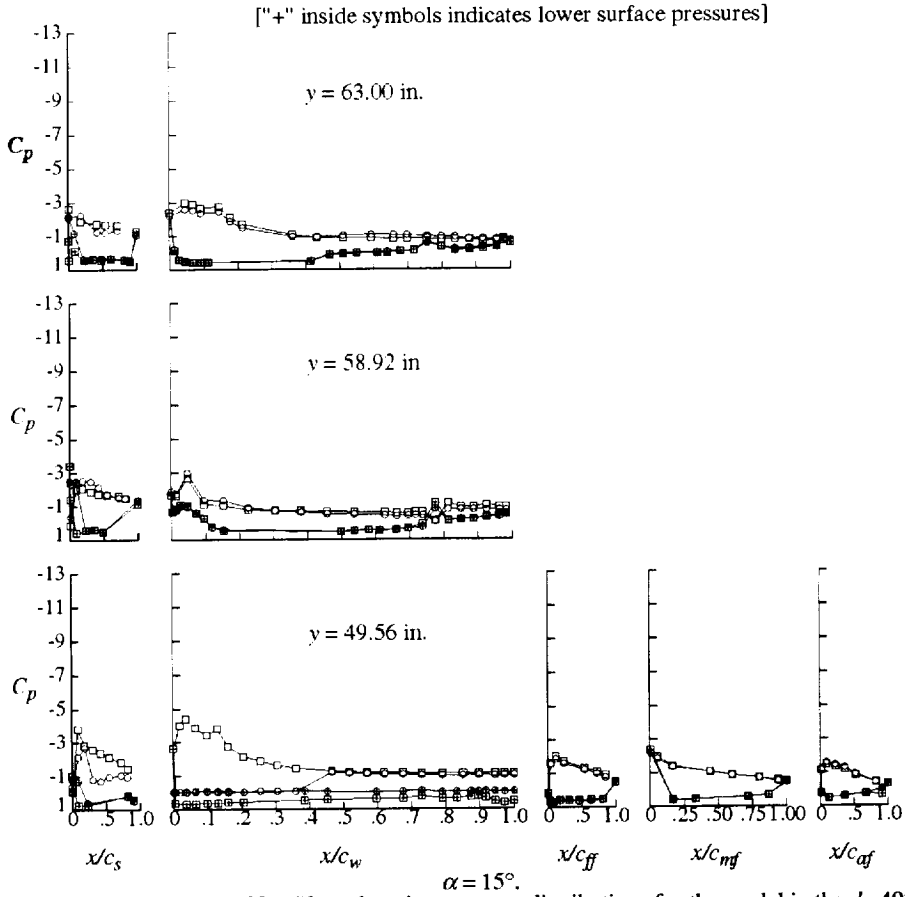

Figure 9 (concluded).—Effects of Ice #2 on the wing pressure distributions for the model in the d_f=40° configuration.

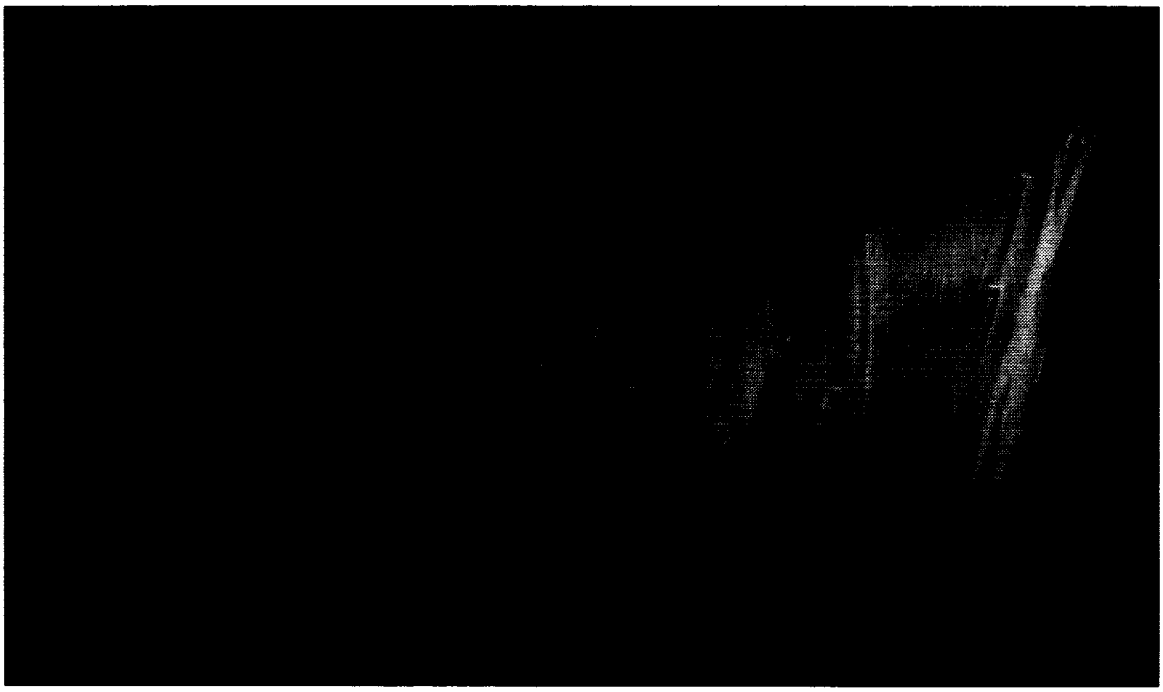

Figure 10.—Main wing flow visualization for no ice, d_f=40°, a=0°, b=0° condition.

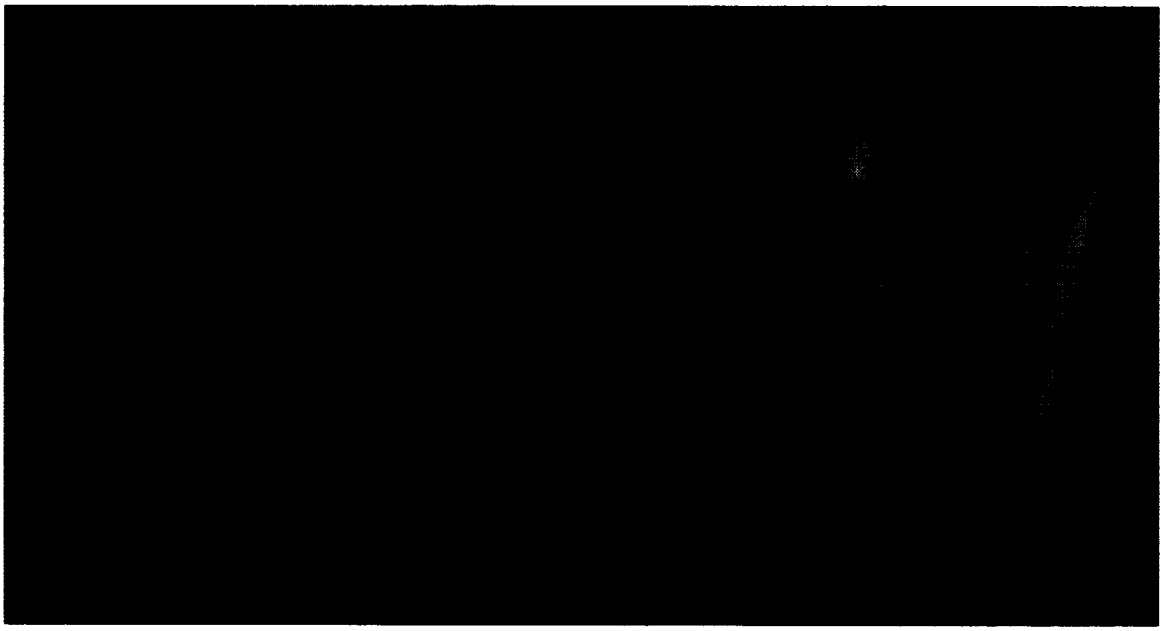

Figure 11.—Main wing flow visualization for ice #2, d_f=40°, a=0°, b=0° condition.

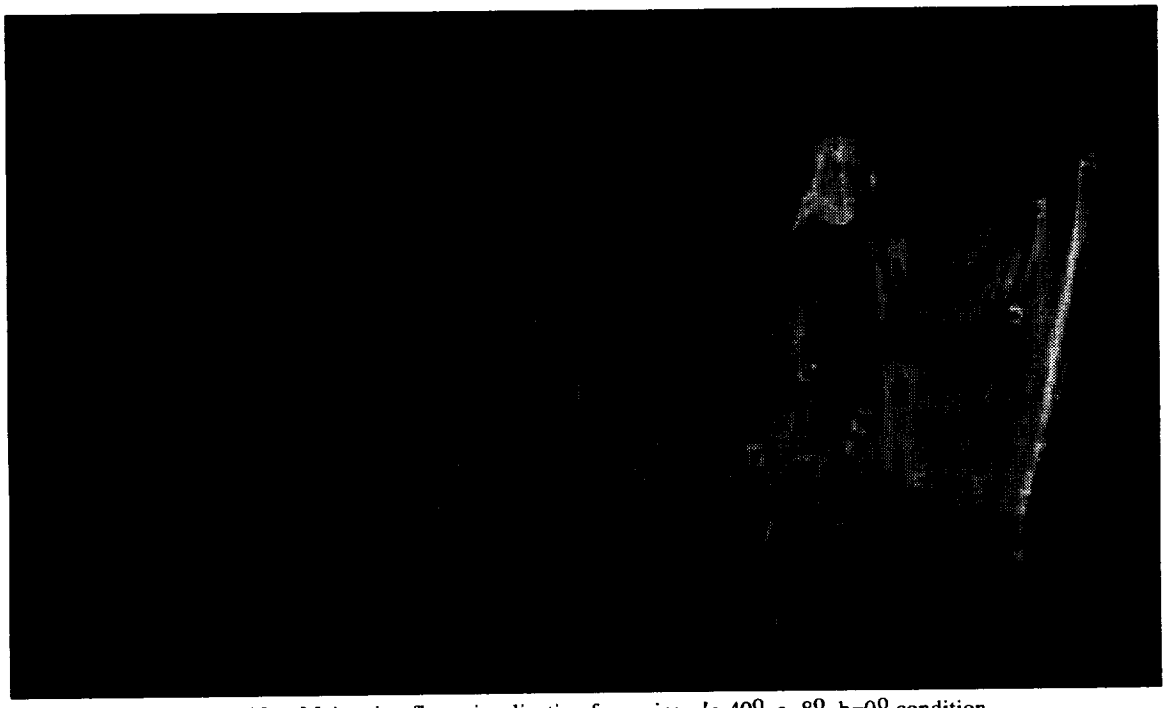

Figure 12.—Main wing flow visualization for no ice, d_f=40°, a=8°, b=0° condition.

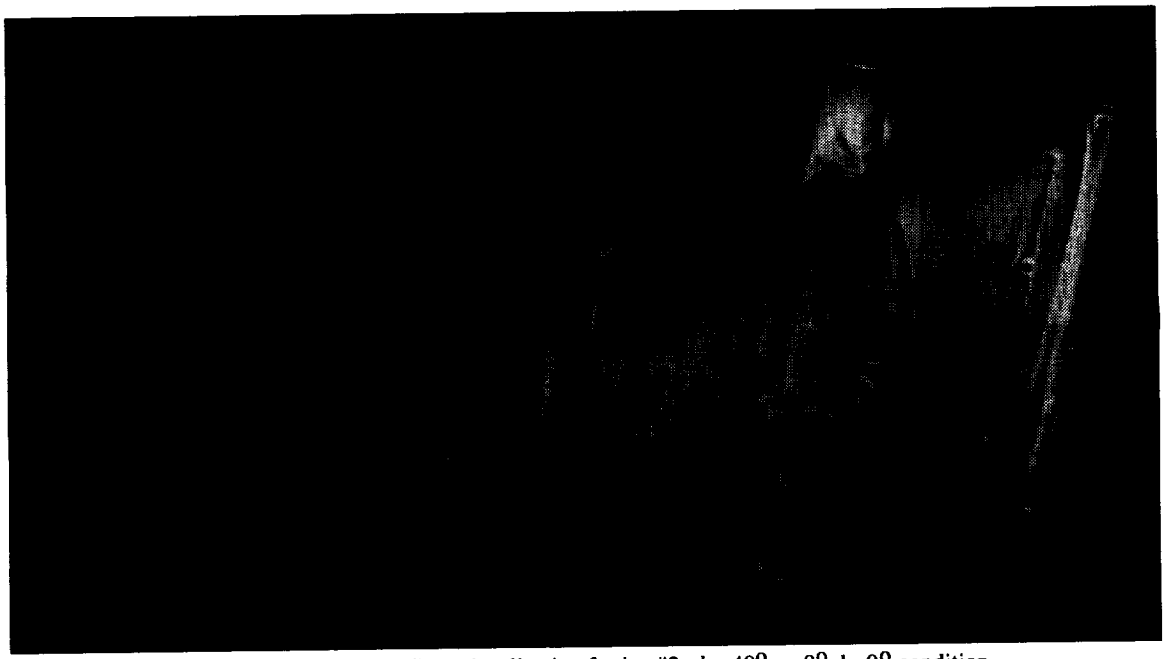

Figure 13.—Main wing flow visualization for ice #2, d_f =40°, a=8°, b=0° condition.

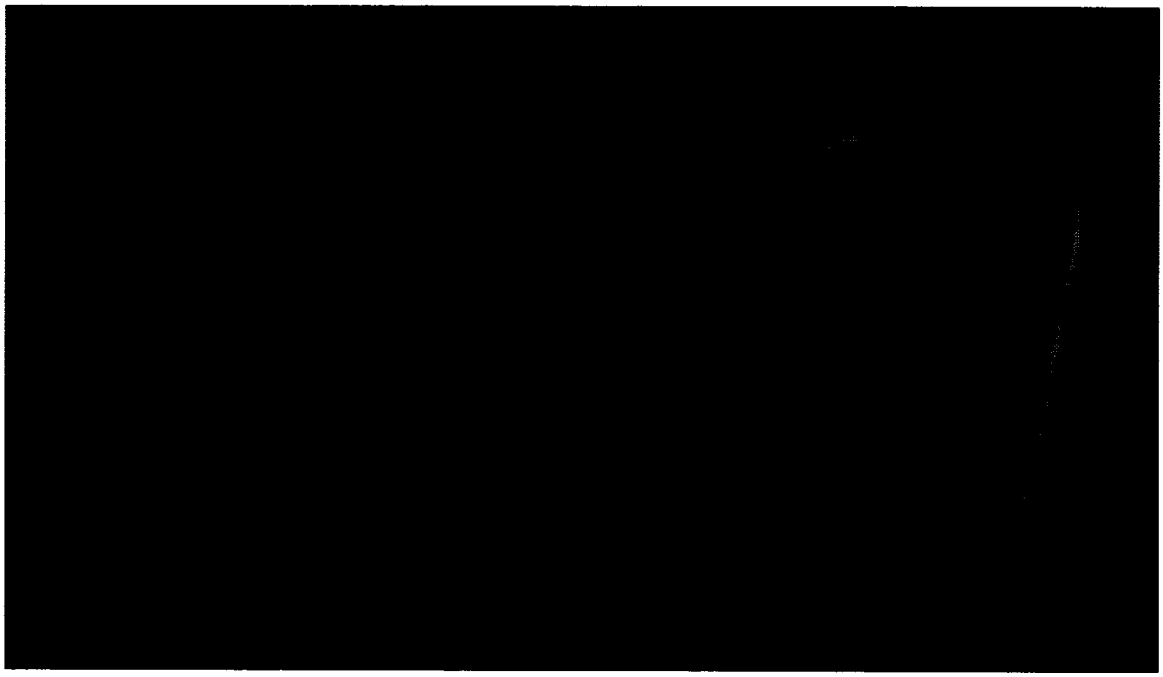

Figure 14.—Main wing flow visualization for no ice, d_f=40°, a=10°, b=0° condition.

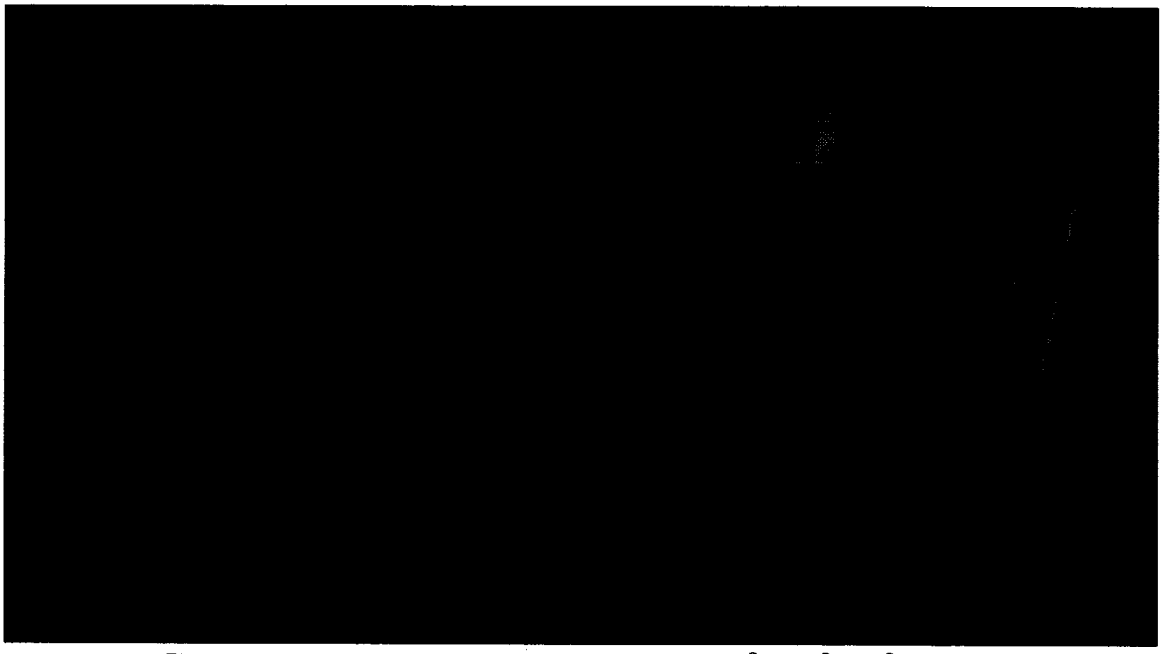

Figure 15.—Main wing flow visualization for ice #2, d_f=40°, a=10°, b=0° condition.

Figure 16.—Main wing flow visualization for no ice, d_f=40°, a=12°, b=0° condition.

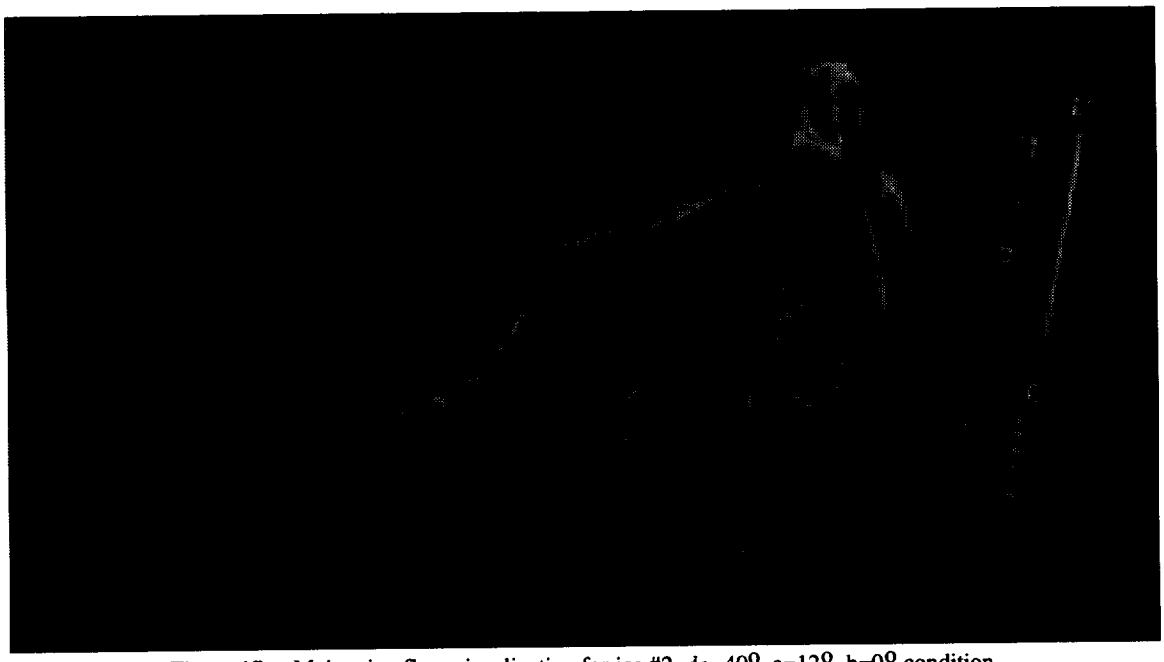

Figure 17.—Main wing flow visualization for ice #2, d_f=40°, a=12°, b=0° condition.

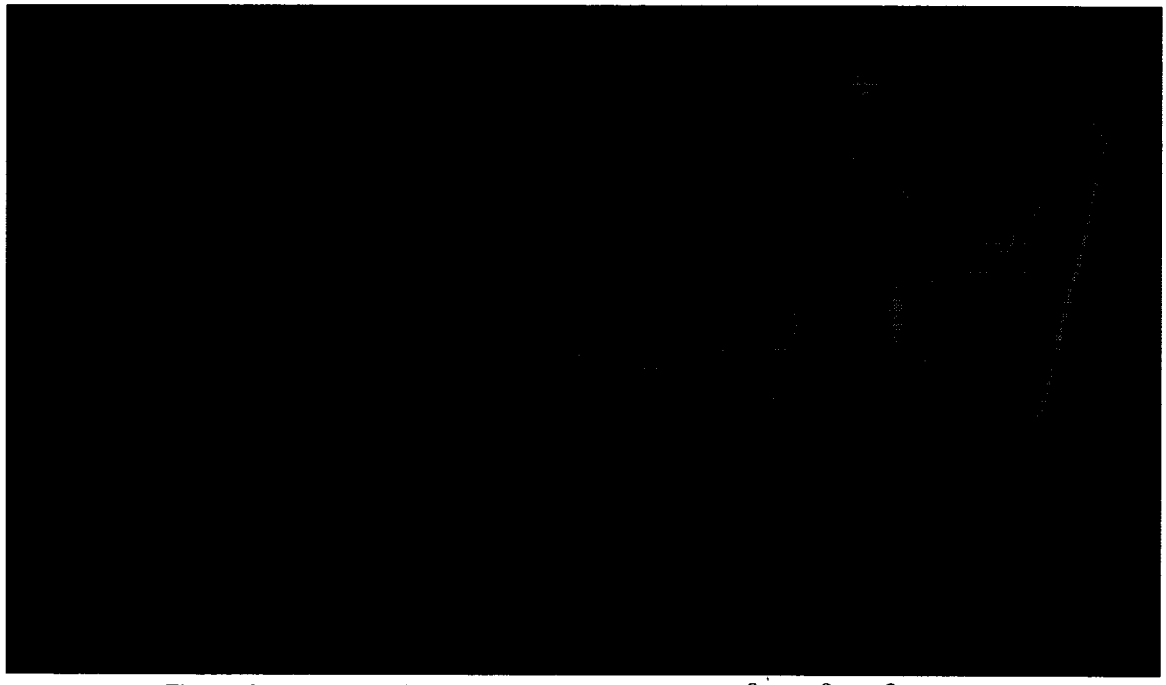

Figure 18.—Main wing flow visualization for no ice, d_f=40°, a=13°, b=0° condition.

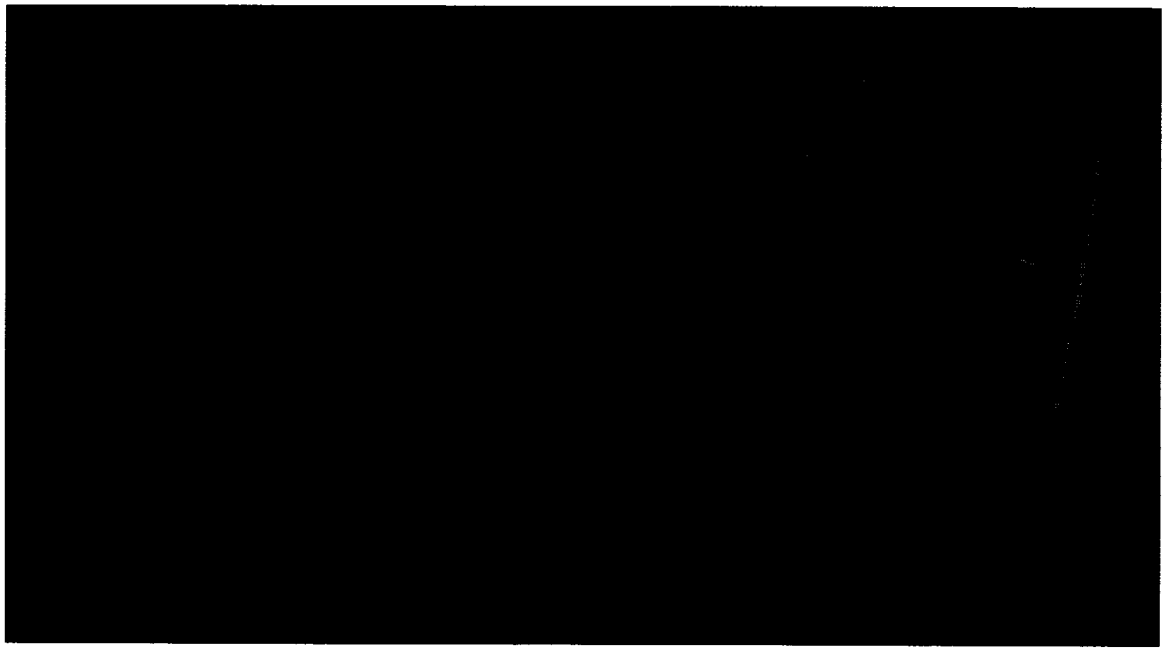

Figure 19.—Main wing flow visualization for ice #2, d_f=40°, a=13°, b=0° condition.

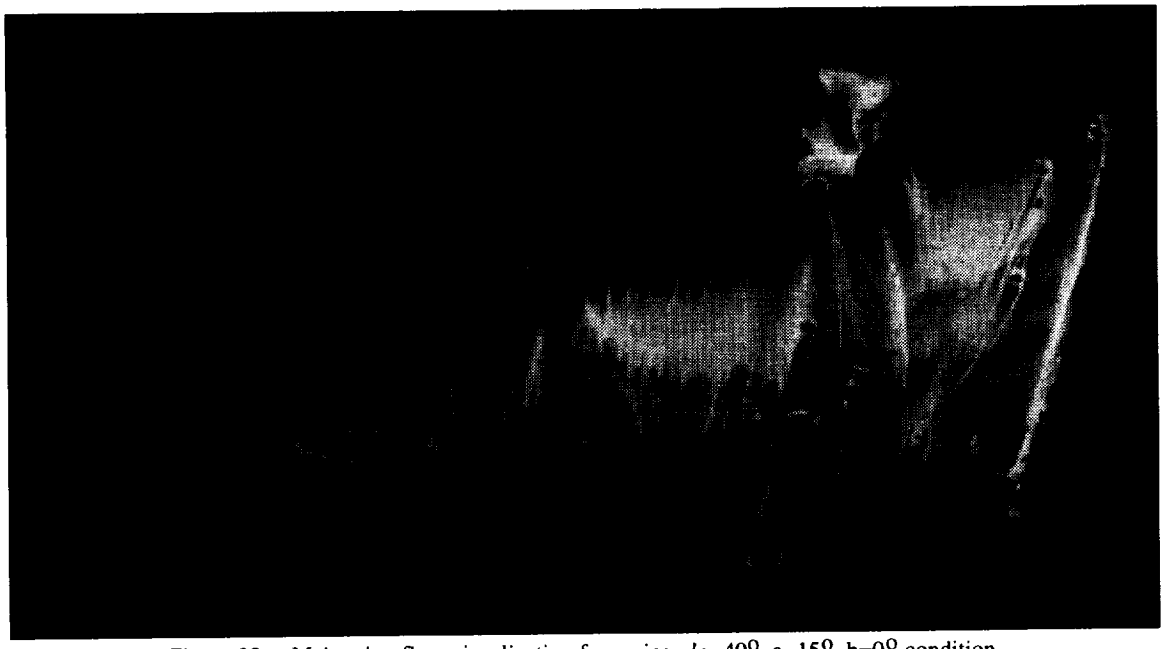

Figure 20.—Main wing flow visualization for no ice, d_f=40°, a=15°, b=0° condition.

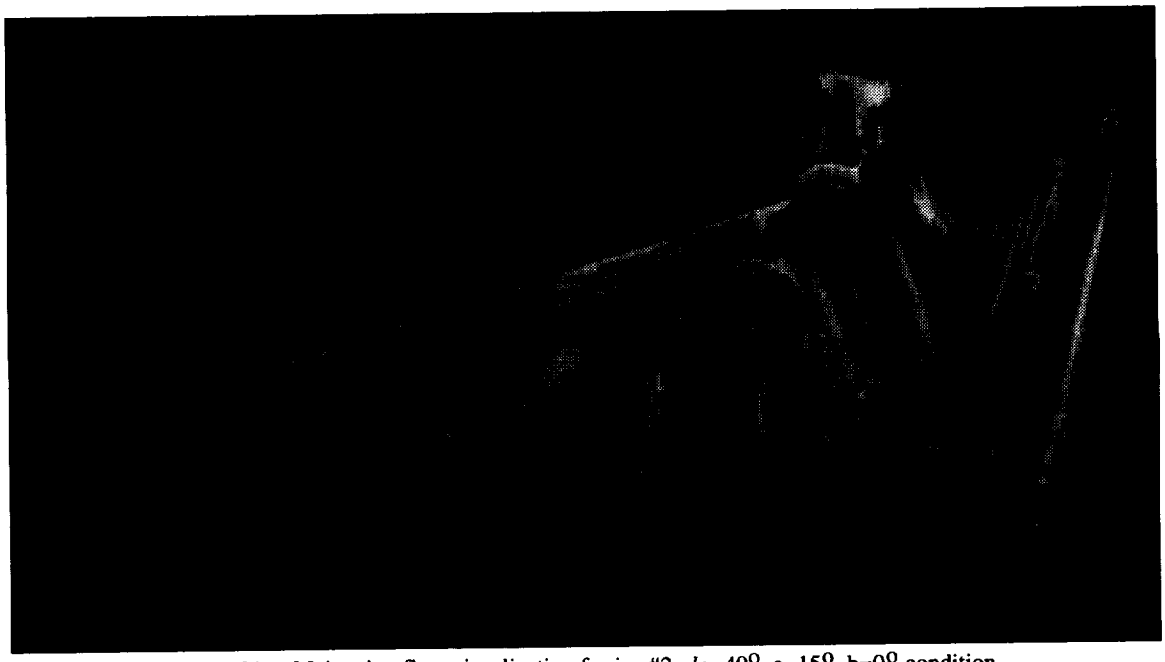

Figure 21.—Main wing flow visualization for ice #2, d_f=40°, a=15°, b=0° condition.

REPORT DOCUMENTATION PAGE

Form Approved
OMB No. 0704-0188

1. AGENCY USE ONLY (*Leave blank*)	2. REPORT DATE	3. REPORT TYPE AND DATES COVERED
	January 1996	Technical Memorandum

4. TITLE AND SUBTITLE

Wind Tunnel Measured Effects on a Twin-Engine Short-Haul Transport Caused by Simulated Ice Accretions

5. FUNDING NUMBERS

WU-505-68-10

6. AUTHOR(S)

Andrew Reehorst, Mark Potapczuk, Thomas Ratvasky, and Brenda Gile Laflin

7. PERFORMING ORGANIZATION NAME(S) AND ADDRESS(ES)

National Aeronautics and Space Administration
Lewis Research Center
Cleveland, Ohio 44135-3191

8. PERFORMING ORGANIZATION REPORT NUMBER

E-10073

9. SPONSORING/MONITORING AGENCY NAME(S) AND ADDRESS(ES)

National Aeronautics and Space Administration
Washington, D.C. 20546-0001

10. SPONSORING/MONITORING AGENCY REPORT NUMBER

NASA TM-107143
AIAA-96-0871

11. SUPPLEMENTARY NOTES

Prepared for the 34th Aerospace Sciences Meeting and Exhibit sponsored by the American Institute of Aeronautics and Astronautics, Reno, Nevada, January 15-18, 1996. Andrew Reehorst, Mark Potapczuk, and Thomas Ratvasky, NASA Lewis Research Center; Brenda Gile Laflin, NASA Langley Research Center, Hampton, Virginia. Responsible person, Andrew Reehorst, organization code 2720, (216) 433-3938.

12a. DISTRIBUTION/AVAILABILITY STATEMENT

Unclassified - Unlimited
Subject Category 03

This publication is available from the NASA Center for Aerospace Information, (301) 621-0390.

12b. DISTRIBUTION CODE

13. ABSTRACT ***(Maximum 200 words)***

A series of wind tunnel tests were conducted to assess the effects of leading edge ice contamination upon the performance of a short-haul transport. The wind tunnel test was conducted in the NASA Langley 14 by 22 foot facility. The test article was a 1/8 scale twin-engine short-haul jet transport model. Two separate leading edge ice contamination configurations were tested in addition to the uncontaminated baseline configuration. Several aircraft configurations were examined including various flap and slat deflections, with and without landing gear. Data gathered included force measurements via an internal six-component force balance, pressure measurements through 700 electronically scanned wing pressure ports, and wing surface flow visualization measurements. The artificial ice contamination caused significant performance degradation and caused visible changes demonstrated by the flow visualization. The data presented here is just a portion of the data gathered. A more complete data report is planned for publication as a NASA Technical Memorandum and data supplement.

14. SUBJECT TERMS

Airport icing; Wind tunnel; Aircraft performance; Flow visualization

15. NUMBER OF PAGES

25

16. PRICE CODE

A03

17. SECURITY CLASSIFICATION OF REPORT	18. SECURITY CLASSIFICATION OF THIS PAGE	19. SECURITY CLASSIFICATION OF ABSTRACT	20. LIMITATION OF ABSTRACT
Unclassified	Unclassified	Unclassified	

National Aeronautics and
Space Administration

Lewis Research Center
21000 Brookpark Rd.
Cleveland, OH 44135-3191